Chapter 2
Fast Computation of the Steady-State Stability Limit

Savu C. Savulescu

Abstract This chapter addresses the theoretical foundation of a field-proven real-time steady-state stability tool (The commercial name of this tool is *Siemens Spectrum Power QuickStab*. The software is owned by Siemens AG, Germany, and is seamlessly integrated with the Spectrum Power SCADA/EMS platform and SIGUARD® Dynamic Security Assessment suite) that quickly and reliably quantifies and visualizes the risk of blackout due to instability. The approach is inspired from Paul Dimo's steady-state stability analysis method and uses the Bruk–Markovic reactive power stability criterion in the REI Nets framework to determine how far the power system is from a state where voltages may collapse and generators may lose synchronism. The technique derives its speed and robustness from Dimo's sound approximations and simplifying assumptions, which are analyzed and substantiated. Metrics that quantify the distance to instability and to the security margin are also discussed, along with innovative tools that extract and visualize essential *information* from the large amount of computational results.

2.1 Introduction

Modern transmission networks must sustain megawatt (MW) transfers that can be quite different from those for which they were planned. This is because energy transactions across multi-area systems may cause parallel flows, excessive network loadings, and low bus voltages. Under certain conditions, such degraded states may lead to blackouts—but how to *quantify* the risk of blackout? How to do it *quickly* in real time, using input from the most recent state estimate and displaying the results before the immediately next state estimation cycle, so that the operator could make *truly online, split-second decisions*? And how to extract *essential* information from large amounts of data and computational results and present it in formats that can be instantly understood and relied upon?

S. C. Savulescu (✉)
Energy Consulting International, Inc., 405 Lexington Avenue, 26th Floor,
New York, NY 10174, USA
e-mail: savu@eciscs.com

S. C. Savulescu (ed.), *Real-Time Stability in Power Systems,*
Power Electronics and Power Systems, DOI 10.1007/978-3-319-06680-6_2,

The industry has taken for granted concepts such as the Available Transfer Capability (ATC), Total Transfer Capability (TTC), and Transmission Reliability Margin (TRM), but was slow to recognize the need to run real-time stability checks after every single state estimation solution and after each market clearing computation.

According to the North American Electric Reliability Corporation (NERC; NERC 1966), the TTC is given by

$$\text{TTC} = \text{Min}\left\{\text{Thermal Limit},\ \text{Voltage Limit},\ \text{Stability Limit}\right\}$$

Thermal and voltage limits can reliably be defined off-line. They are predictable and can even be briefly violated. But how about "stability limits?" NERC's Policy 9 (NERC 2000) requires reliability coordinators to compute "stability limits" for the current and next-day operation processes to "foresee whether the transmission loading progresses or is projected to progress beyond the operating reliability limit." This is easier said than done, for detecting thermal and voltage violations is relatively straightforward, whereas defining, quantifying, and computing "stability limits" is an altogether different proposition, especially if it has to be done online.

In order to qualify for real-time deployment, the stability software must, of course, be fast and reliable but, in addition, it should also provide the *ability to identify, quantify, and visualize the stability limits,* as opposed to just assessing whether a given condition is stable or unstable.

Many, if not most, stability tools available until a few years ago, would *not* meet both these requirements. They "determine whether a given condition is stable or unstable, [but] have not been efficient in quickly and automatically determining the stability limits" (Kundur 1999).

Actually, Professor Kundur's statement was an understatement, in the sense that the term "stability limit" was used without having been explicitly defined or mathematically quantified—not only in this widely quoted reference but also in the literature available at that time. Common sense suggests that if conventional techniques can neither quantify the stability limit, or limits, nor perform split-second computations, an alternate paradigm, perhaps entailing simplifications, should be used—provided that such simplifications would come from sound assumptions and lead to algorithms that are fast and provide dependable answers as well.

Indeed, a method that meets these requirements was developed in Europe in the early 1960s by Paul Dimo (Dimo 1961, 1975) and introduced in the USA in the 1990s (EPRI 1992, 1993; Savulescu et al. 1993; Erwin et al. 1994). It quickly became obvious that, if taken from the drawing board to the real life, this approach does have the potential to overcome the real-time stability challenge. As a result, practical features were incorporated and a commercial-grade stability tool was developed and, then, deployed in actual power system control centers (Gonzalez 2003; Avila-Rosales et al. 2004; Savulescu 2004; Tweedy 2004; Avila-Rosales and Giri 2005; Vergara et al. 2005a; Campeanu et al. 2006; Virmani et al. 2007; Vickovic et al. 2009; Arnold et al. 2009; Eichler et al. 2011; Stottok et al. 2013).

The subsequent sections of this chapter:

- Discuss the general background
- Address the benefit of approaching the real-time stability problem through the steady-state stability prism
- Review the mathematical foundation of Dimo's steady-state stability analysis method
- Briefly close the gap from theory to implementation and review a set of user-friendly visualization tools inspired from the otherwise cryptic Nodal Images originally introduced by Dimo half a century ago.

2.2 General Background

2.2.1 In Search of the Stability Limit

Conceptually, the "stability limit" is a local property of the system state vector: For each new solution of the system of equations that describe the system state, there is a new stability limit. For example, the stability conditions change when static capacitors and shunt reactors are switched. Likewise, transformer tap changes, line outages, load variations, and generator trips affect the distance to instability. To further complicate things, the stability limit also depends upon the path followed to approach it: different search paths may lead to different stability limits.

Simply stated, stability limits exist, are not fixed, and change with the total MW system grid utilization,[1] bus voltage profile, network topology, and the path followed to approach them. It is precisely because of this changing nature of the stability limits that they must be recalculated as often as possible—assuming, of course, that a *metric* has previously been defined so that such stability limits could be *quantified*.

Furthermore, instability develops instantly and leaves no time to react, so, in addition to the need of indices that quantify the distance to instability, the ability must also be provided to rapidly recompute the underlying indices for each new system state, after each state estimate, and after each load flow.

2.2.1.1 Transient and Voltage Stability Limits[2]

The main directions investigated in the industry during the past two decades point primarily at transient stability and voltage stability. On the *transient stability* venue,

[1] When the system is *importing* power, the total MW system grid utilization is calculated by summing up the total MW generation with the total imported MW; when *exporting* power, the total MW system grid utilization is the total generated MW. In other words, this number shows how many MW are currently "circulating" in the transmission system.

[2] Portions of this section have been reprinted with permission from Savulescu, S.C. (2004).

much work was done to develop "transient stability indices" aimed at computing the "degree of stability"[3] (Kundur 1999).

Regardless of the specific details, these methods follow similar scenarios:

- Start with a base case and a postulated major contingency
- Derive a "severity index" for this contingency
- Compute new power flows for successively degraded states
- Repeat the sequence until either the load flow diverges or an unstable case has been obtained

Their limitations are similar, too:

- Computational burden, which some authors attempted to alleviate by
  - merging all the machines into an equivalent generator, which makes it impossible to identify the dangerous generators and their impact on the system stability conditions
  - using the infinite bus assumption, i.e., implying that voltages are constant, although, in real life, the bus voltages drop when the power system is approaching a state where instability might occur
- Need to examine a huge set of disturbance scenarios, thus further escalating the computational complexity

Voltage stability, also known as load stability (Venikov 1977; Barbier and Barret 1980; Vournas et al. 1996), refers to the maximum MW that can be transferred to a given load bus prior to the occurrence of voltage collapse. But in order to develop a *system-wide* view from such *bus-oriented* calculations, the procedure must be repeated for all the load buses, which becomes computationally expensive for large system simulations.

A more serious limitation comes from the load model. If the load is modeled as constant impedance, the bus MW initially increases up to a maximum, then it gets smaller and *dual power states* (same power at different voltages) are obtained (Ionescu and Ungureanu 1981)—and this is what actually causes the "nose" pattern of the *P–V* curves. But dual states *cannot* happen in real life, and the validity of any *P–V* curve drawn on this basis is questionable.

Let us mention en passant the inadequacy of "assessing stability" by running load flows at successively increased load levels and stopping when the load flow diverged. While it is true that Newton–Raphson load flows diverge near instability (Venikov et al. 1975), they may diverge for many reasons. Sauer and Pai (Sauer and Pai 1990) have demonstrated that "for voltage collapse and voltage instability analysis, any conclusions based on the singularity of the load-flow Jacobian would apply only to the voltage behavior near maximum power transfer. Such analysis would not detect any voltage instabilities associated with synchronous machines characteristics and their controls."

[3] With all the respect due to Professor Kundur, this often-quoted paper uses the term "degree of stability" as an a priori concept but neither defines nor quantifies it.

Perhaps the most significant challenge is the representation of generators, which *must* be taken into account (Barbier and Barret 1980; Ionescu and Ungureanu 1981; Sauer and Pai 1990; Kundur and Morison 1993). In the world of continuation load flows, this is a classic catch-22 situation: If the generator reactances *are not* included in the power system model, the ensuing load-flow calculations are meaningless from the point of view of stability; if the machine reactances *are* represented, the values of the generators' internal electromotive force (emf), which are typically much higher than 1.0 pu, would cause the load-flow calculations to diverge.

One way out of this dilemma is to represent the machines in detail, via transfer functions, in which case, much more complex algorithms would have to be deployed (EPRI 1992; Morison et al. 2004), thus significantly increasing the computational burden—or, even better, to change gears entirely and move into the much more promising realm of steady-state stability.

2.2.1.2 The Steady-State Stability Connection

Steady-state stability[4] is the stability of the system under conditions of gradual or relatively slow changes in load (Crary 1945). Accordingly, the steady-state stability limit (SSSL) of a power system is "a steady-state operating condition for which the power system is steady-state stable but for which an arbitrarily small change in any of the operating quantities in an unfavorable direction causes the power system to lose stability" (IEEE 1982; Navarro-Perez and Prada 1993).

Voltage collapse, units losing synchronism, and instability caused by self-amplifying small-signal oscillations are all forms of steady-state instability. Empirically, the risk of steady-state instability[5] is associated with low real/reactive power reserves, low voltage levels, and large bus voltage variations in the presence of small load or generation changes.

Recurring "temporary faults" where breakers trip without apparent reason, i.e., are disconnected by protection without being able to identify the fault, might also be indicative of steady-state instability. Breaker trips can happen when loads increase due to "balancing rotors" of generators that trip near instability and then get back in synchronism. In some cases, "the resynchronization happened after the rotor turned 360°, which, in turn, led to lower voltages" (Dimo 1968).

The possibility of operating for a very short time in an unstable operating state and resynchronization due to the action of fast voltage controllers has been known for a long time (Magnien 1964). Also, according to the same report, "any network

[4] By "steady-state stability," we refer to the *classical concept* described by Crary (1945), Venikov (1977), IEEE (1982), and Anderson and Fouad (1990), as opposed to "small-signal stability," as it is understood nowadays (IEEE/CIGRE 2004).

[5] Throughout the remainder of this chapter and, in general, in the literature that addresses Dimo's concepts and related stability applications, "steady-state instability" actually refers to "aperiodic steady-state instability" and assumes that self-amplifying system oscillations either do not occur or have been prevented by the existence of power system stabilizers.

that meets the steady-state stability conditions can withstand dynamic perturbations and end in a stable operating state" (Magnien 1964).

The SSSL spans a promising landscape. First and foremost, it is *quantifiable,* as shown in the Sect. 3.4.1. Then, it *does* represent an operating limit, in the sense that operating conditions *immediately* below SSSL become unstable if a small change in any of the operating quantities in an unfavorable direction takes place.

Simplicity is another benefit: For a given topology, load and generation conditions, and reactive compensation scenario, the SSSL is simply the total MW grid utilization of the transmission system, including both internal generation and tie-line imports, where voltages may collapse and units may lose synchronism.

Furthermore, although the SSSL depicts an unsafe state, the algorithm used to compute it can be reversed to determine a *security margin,* thus potentially eliminating the need to perform dynamic simulations, if the total base case MW system grid utilization is below such "security margin" (Moraite et al. 1966).

On this basis, a metric of system-wide indices emerges and provides for quantitatively assessing "how far from SSSL" and "how safe" is a given operating state. One pillar of this metric is the *steady-state stability reserve* index; the other one is the *security margin* index. Both these indices change, and need to be computed, for each new system state—and, together, they span the concept of *stability envelope,* as shown in the following section.

2.2.2 *Transient stability limit , total transfer capability, and the Stability Envelope*

A Transient Stability Limit (TSL) also exists (Navarro-Perez and Prada 1993), but, as opposed to SSSL, and because of the computational algorithms and strategy used to detect transient instability, it is not quantifiable through a specific formula. In order to find it, transient stability simulations would have to be performed for each potential fault starting from a base case scenario and continuing with a sequence of successively degraded operating states until the first unstable state has been found.

The intrinsic computational complexity and the large number of credible contingencies render such a problem practically unsolvable.

However, intuition suggests (Fig. 2.1) that:

- For a given set of relay settings, TSL depends, just like the SSSL, upon topology, voltage levels, and total MW system grid utilization.
- For any system state, SSSL and TSL are interrelated and move in the same direction: if SSSL is high, TSL is also high, and vice versa.

In the past, empirical values approximating the *TSL/SSSL ratio* have been used to compute a "safe" MW system grid utilization, referred to as *security margin,* such that, for any system state with a steady-state stability reserve smaller than it, no contingency, no matter how severe, would cause transient instability (Moraite et al. 1966; Dimo et al. 1971).

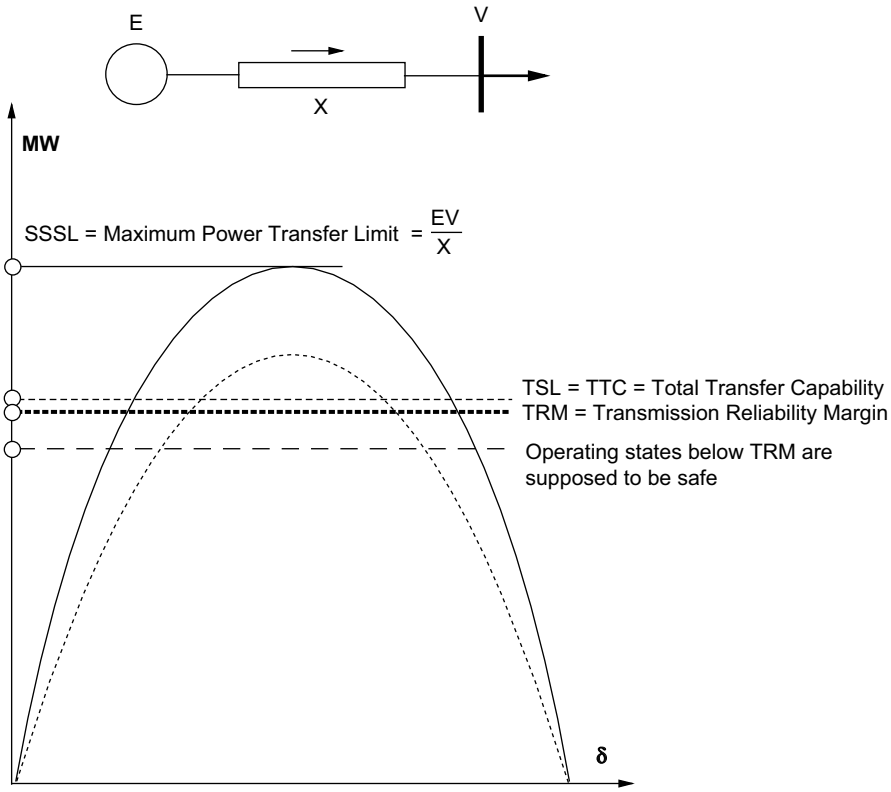

Fig. 2.1 TTC and TRM seen from the steady-state stability perspective

The security margin, which is expressed as a percentage of the steady-state stability reserve, depends upon topology, loads, generators, and reactive compensation. It changes from system to system and, for a particular power system, must be reassessed periodically and for alternate operating scenarios.

For example, extensive studies and operational experience with the Romanian power system, as it was in the 1960s and 1970s, led to setting the security margin at 15% for normal operating conditions and 8% for contingency cases (Dimo et al. 1971).

We do not know if a mathematical formula relating TSL and SSSL can be developed analytically, but the empirical approach described in Vergara et al. (2005a) can be expanded to build the following heuristic:

1. Start with a base case load flow for peak load conditions and compute the SSSL and related security margin.
2. Run an extensive suite of transient stability simulations. If no instability has been detected, go to Step 5. If at least one contingency (fault) case was found to be unstable, go to Step 3.

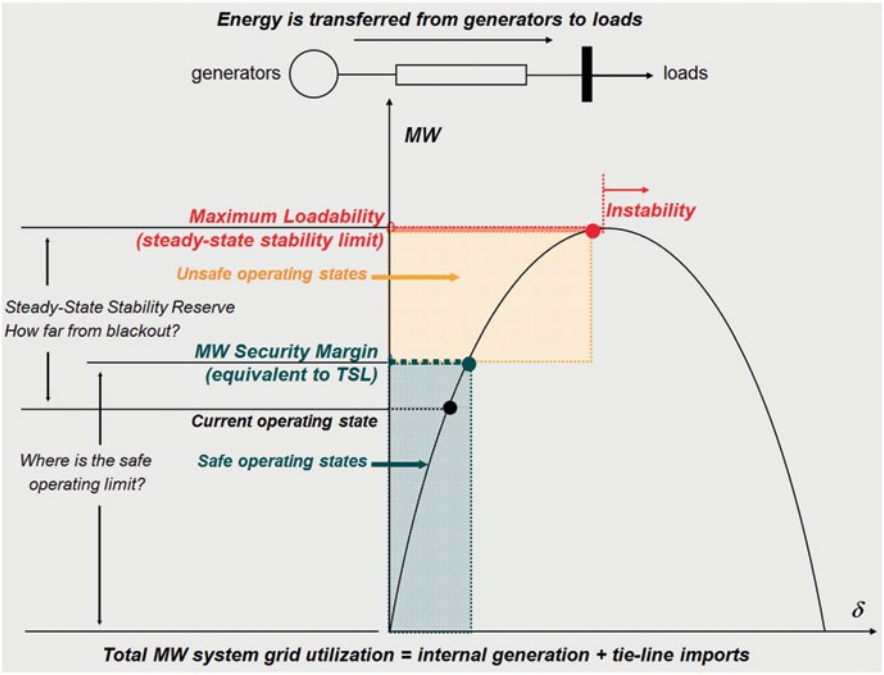

Fig. 2.2 The "stability envelope"

3. Use the security margin MW generation schedules from Step 1 to calculate a new base case load flow.
4. For the load flow computed in Step 3, run an extensive suite of transient stability simulations.
5. If no instability has been detected, repeat Step 4 for successively increased MW levels until at least one contingency causes transient instability. The steady-state stability reserve for the immediately precedent state is the security margin of the system under evaluation.
6. If the Step 4 calculations detected at least one contingency (fault) that would cause instability, build a new load-flow case for a slightly reduced load level and repeat the transient stability checks. If no instability has been detected, recalculate the SSSL and the steady-state stability reserve, which is the security margin of the system under evaluation.

The MW value of the security margin represents a "safe system MW loading limit" that can be interpreted as a *stability envelope* (Fig. 2.2).

Assuming there are no thermal violations, i.e., if the TSL in Fig. 2.2 is the same as NERC's TTC, the stability envelope corresponds to NERC's definition of TRM and is obtained as follows:

- *First*: Starting from a state estimate or solved load flow, determine the steady-state stability reserve, i.e., the distance to SSSL.
- *Subsequently*: For a postulated *x*% value of the security margin, determine the corresponding safe system MW loading below the SSSL.

The computation of the steady-state stability reserve can be accomplished both by detailed analysis and via approximate methods. Detailed steady-state stability methods have been proposed (Arie et al. 1973) but do not seem to have been actually implemented.

By contrast, approximate methods, if fast and reasonably accurate, are attractive both for real-time and for off-line stability checks. Dimo's technique belongs to this category. At the time when it was introduced, it was used in operations and long-range planning. Its recent extensions improved the computational speed and robustness and, with the newly added visualization capabilities, it has been implemented and successfully used in real time for several years. This topic is addressed in the following section.

2.3 Overview of Paul Dimo's Steady-State Stability Analysis approach

2.3.1 General

Paul Dimo's methodology is predicated on the following major concepts:

- Short-circuit current's network transformation that leads to an REI Net
- Vectorial representation of the short-circuit currents on a Nodal Image
- Use of the reactive power voltage and steady-state stability criterion in conjunction with the Nodal Image
- ase-worsening procedure for computing successively degraded power system states when performing system-wide stability analysis

2.3.2 Short-Circuit Currents and REI Nets

Let us consider a typical power system network (Fig. 2.3) and let I, Y and V be the vector of complex injected currents, matrix of complex nodal admittances, and vector of complex bus voltages. The steady-state conditions of this network are given by

$$I = YV \tag{2.1}$$

$$\underline{S}_k = \underline{I}^*_k \underline{V}_k \tag{2.2}$$

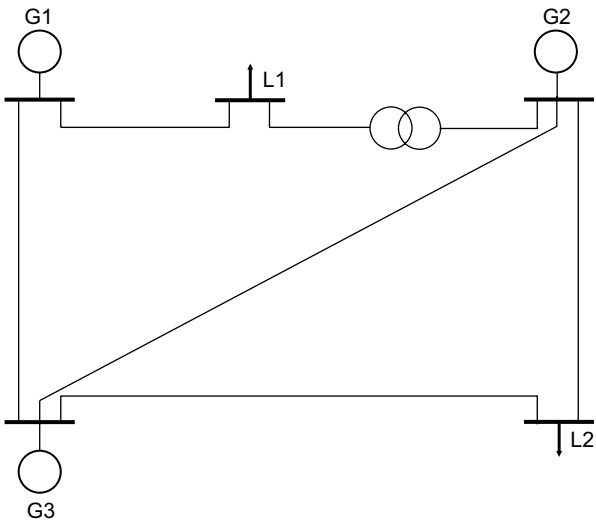

Fig. 2.3 Typical power system network

where S_k is the complex power injected into the bus k, I_k^* is the conjugate of the complex current injected into the bus k, and V_k is the complex bus voltage of the bus k. The load buses are numbered sequentially after the generator buses as follows: $1 \ldots m \ldots G$ generator buses and $i \ldots N$ load buses, where, for convenience, $G+1$ was noted as i.

The standard approach to evaluate the system generators' impact on a specific load bus, let us say the load bus L_1, is to linearize all the other load buses, i.e., replace the injected currents with constant admittances, include these admittances in the diagonal term of Y, and perform Gauss–Seidel eliminations to reduce the system to a network encompassing only the $1 \ldots G$ generator buses and the load bus L_1. Figure 2.4 shows how the power system network depicted in Fig. 2.3 is "seen" from the load buses L_1 and L_2.

This process, which allows *seeing* the system generators from any load bus in the power system network, has been used extensively in the voltage stability literature, e.g., (Barbier and Barret 1980) and is known as the *short-circuit currents transformation*. The currents that flow from generators to the load bus in the reduced network are none other than the currents from the bottom equation obtained from Eqn (2.1) after eliminating the linearized buses (Fig. 2.5).

If the bus voltages of the generator nodes are the internal voltages of the generators applied at the ends of their internal reactance (synchronous, transient, etc.), then the two components of the current I_i in Fig. 2.5 are short-circuit currents (permanent, transient, etc.):

- $\Sigma Y_{im} E_{im}$ is the symmetric threephase short-circuit current flowing into the bus i in the case where the voltage $V_i = 0$
- $(\Sigma Y_i + Y_{io}) V_i$ is the "no-load short-circuit current" of the bus i and corresponds to the short-circuit current at the bus i if the load current was equal to zero before the short circuit.

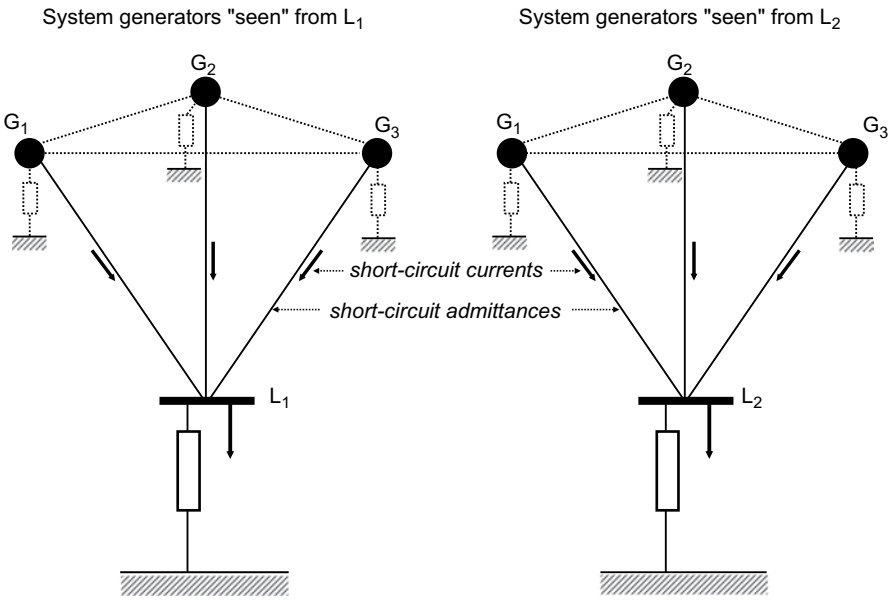

Fig. 2.4 System generators "seen" from load buses

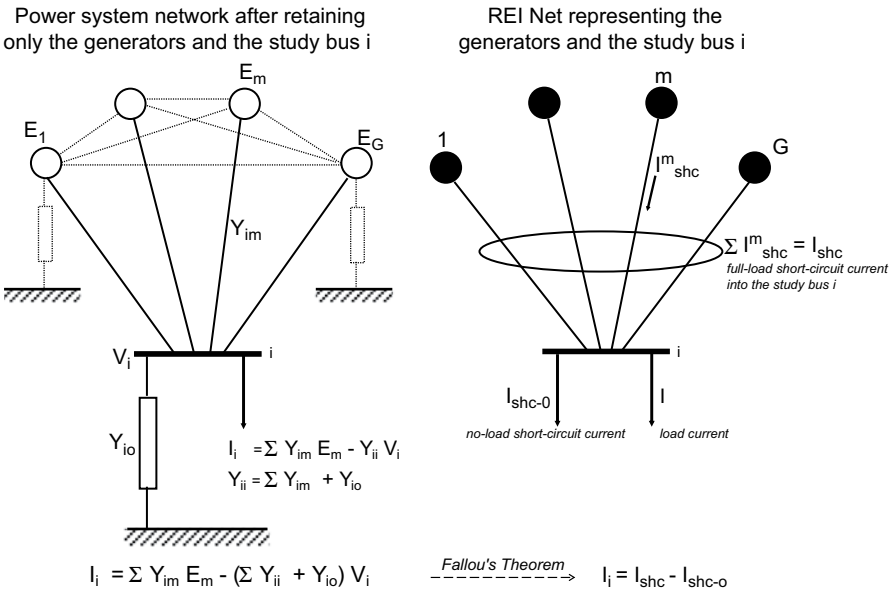

Fig. 2.5 Short-circuit currents and short-circuit admittances. The REI Net

This radial network of short-circuit admittances, or *REI Net,*[6] in Dimo's terminology (Dimo 1962), is built for a reference state, or base case, for which a load-flow computation has been performed and converged. The base case may depict a peak load case or some other system state involving certain particular features, e.g., high percentage use of hydraulic power, single or multiple line and/or generator contingency, and so on.

The study-bus retained in the model may be actual or fictitious. If it is an *actual load bus* connected *directly* to generators, the machines are "seen" via the short-circuit currents that flow across the actual admittances between generators and load. If the study-bus is an *actual load bus* connected to generators through a typical transmission network, the generator buses are "seen" via short-circuit currents flowing across short-circuit admittances between generators and the load bus.

If the study-bus is a *fictitious load center,* i.e., an equivalent bus where all the system loads have been aggregated by inserting a Zero Power Balance Network and reducing the system to the particular type of REI Equivalent shown in Fig. 2.6, the machines are "seen" via the short-circuit currents that flow across short-circuit admittances between generators and the fictitious load bus.

The generator buses may correspond to either actual synchronous machines or *virtual generators* introduced to model tie-line imports, static VAr compensators (SVCs), Direct Current (DC) injections, etc. It must also be strongly emphasized that in the model built for the purpose of assessing stability, as opposed to a conventional REI Equivalent, *the machines, either real or virtual, must be represented explicitly, and should not be merged into an equivalent generator*.

The REI Net, without introducing any approximations, allows "seeing" the power system network from any bus, either real or fictitious, radially connected with generators via admittances, either actual, i.e., internal generator admittances, or virtual, i.e., short-circuit admittances. As such, it provides a certain amount of information, although rather limited, about the base case for which the short-circuit admittances have been computed.

For example, the module of a short-circuit admittance gives a preliminary indication about the effect of the associated generator on the state of the study-bus. Since, for normal states, the voltages E_m may vary only within a narrow range around the nominal value, it is the short-circuit admittance, i.e., the admittance of the radial branch and the angle across it that have the main impact. Actually, this is a simple way to identify generators and tie-line injections that are negligible when seen from a study bus and to recognize system areas whose impact on the study-bus is significant. The short-circuit admittances' ability to visualize how significant the machines are as seen from a load bus has also been noted by other authors, e.g. Barbier and Barret (1980).

[6] The REI Net is quite different from the so-called REI Equivalent. The former is a radial network of short-circuit admittances that connect the generators to a specific bus, whereas the latter is a reduced model of the power system where the generators have been aggregated into one or several equivalent generators and the loads have been aggregated into one or several equivalent load centers (Dimo 1968, 1975; Tinney and Powell 1977; DyLiacco et al. 1978; Wu and Narasimhamurti 1979; Oatts et al. 1990; Savulescu 1981).

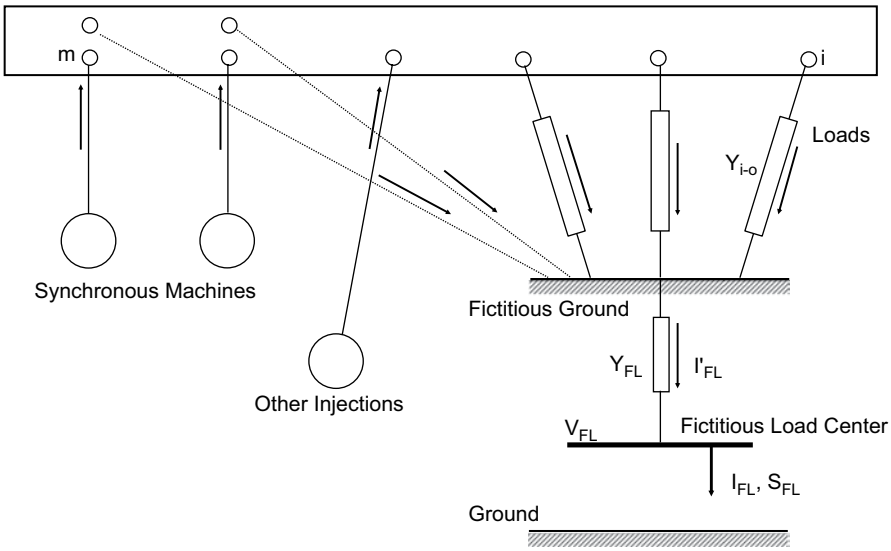

Fig. 2.6 Dimo's Zero Power Balance Network used to build a fictitious load center

We will return to this topic in Sect. 4.2.2. For the moment, let us just say that the short-circuit admittances can help understand the structure of the transmission system, but not more than that. It is only when the REI Net is associated with its "nodal image" that a large amount of meaningful information can be obtained by simple "visualization."

2.3.3 The Nodal Image

The Nodal Image of a bus, either actual or fictitious, is a diagram that shows in detail the short-circuit currents that flow from generators towards that bus across the short-circuit admittances. It is a *vectorial* representation of the short-circuit currents in a system of coordinates defined as follows:

- The ordinate axis is in the direction of the active current I_w.
- The abscissa axis is in the direction of the reactive current I_d.

We will illustrate this concept in two steps—first, an elementary Nodal Image of a synchronous machine connected to a load, then a generalized Nodal Image that can be used to depict the state of any network as "seen" from any actual or fictitious bus.

Let us consider a generator with internal emf and impedance equal to E and Z, respectively,connected at full load to a bus where the voltage has the value V and its phasors are used for reference (Fig. 2.7).

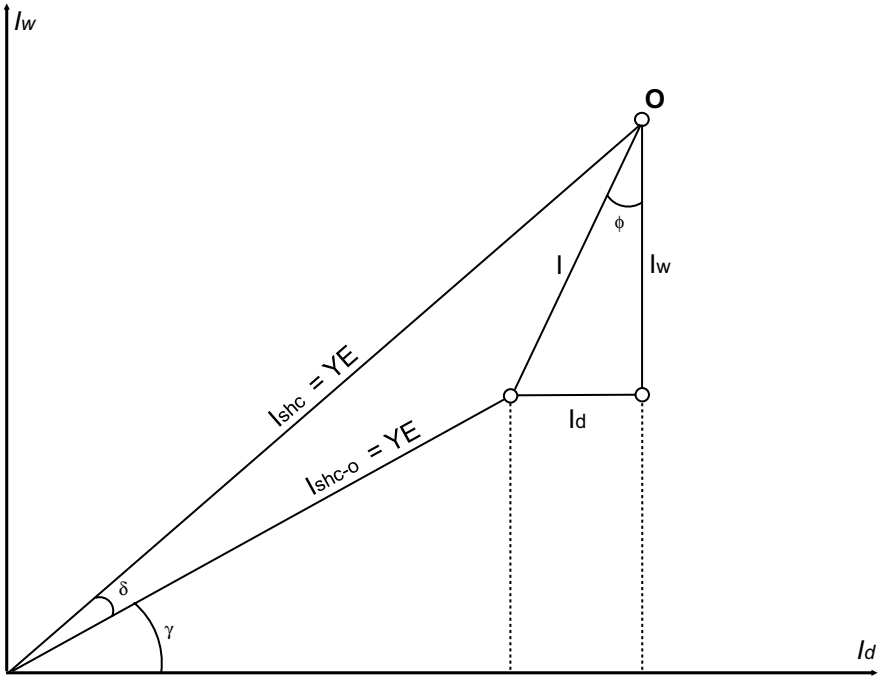

Generator (emf = E) injects the current I into the bus O (bus voltage module = V)

I_{shc} = full-load short-circuit of the generator

$I_{shc\text{-}o}$ = no-load short-circuit of the generator

δ = angle between E and V, where V is used as reference

Fig. 2.7 Nodal Image of a synchronous machine connected to a load bus

The symmetric threephase short-circuit current of the generator is given by

$$\underline{I}_{shc} = \frac{\underline{E}}{\underline{Z}} = \underline{Y}\underline{E} \tag{2.3}$$

If the machine was functioning in no-load conditions prior to the short-circuit, its short-circuit current would be given by

$$\underline{I}_{shc-0} = \frac{\underline{V}}{\underline{Z}} = \underline{Y}\underline{V}, \tag{2.4}$$

and with the notation

$$\tan \varphi = \frac{X}{R} \tag{2.5}$$

we have $Z \mid \varphi$ and $Y \mid \varphi$.

By taking V as phase origin and noting with δ the angle between E and V, the full-load current of the machine can be expressed as:

$$\underline{I} = (E\underline{\lfloor \delta} - V)Y\underline{\rfloor -\varphi}. \tag{2.6}$$

The complex power on the machine's terminals is given by

$$P + jQ = (E\underline{\lfloor -\delta} - V)VY\underline{\rfloor \varphi} = EVY\underline{\lfloor \varphi - \delta} - V^2 Y\underline{\rfloor \varphi}. \tag{2.7}$$

$$P = YEV\cos(\varphi - \delta) - YV^2\cos\varphi \tag{2.8}$$

$$Q = YEV\sin(\varphi - \delta) - YV^2\sin\varphi. \tag{2.9}$$

With the notations $\gamma = 90^\circ - \varphi$ and $\tan\gamma = \dfrac{R}{X}$, we get:

$$P = YEV\sin(\delta + \gamma) - YV^2\sin\gamma \tag{2.10}$$

$$Q = YEV\cos(\delta + \gamma) - YV^2\cos\gamma. \tag{2.11}$$

The real, or "watted," and reactive, or "de-watted," components of the generator currents are given by

$$I_{\mathrm{w}} = YE\sin(\delta + \gamma) - YV\sin\gamma \tag{2.12}$$

$$I_{\mathrm{d}} = YE\cos(\delta + \gamma) - YV\cos\gamma, \tag{2.13}$$

respectively, and since YV and YE are the moduli of the of the no-load and full-load short-circuit currents of the generator, respectively, we obtain:

$$I_w = I_{shc}\sin(\delta + \gamma) - I_{shc-0}\sin\gamma \tag{2.14}$$

$$I_d = I_{shc}\cos(\delta + \gamma) - I_{shc-0}\cos\gamma. \tag{2.15}$$

The general case of G generators connected to a load bus, either actual or fictitious, through short-circuit admittances is illustrated in Fig. 2.8.

Simple vectorial algebra manipulations result in the following equations:

$$\Sigma I_{wm} + \Sigma I_{shc-0m}\sin\gamma_m = I_w + \Sigma I_{shc-0m}\sin\gamma_m = \Sigma_{shcm}\sin(\delta_m + \gamma_m) \tag{2.16}$$

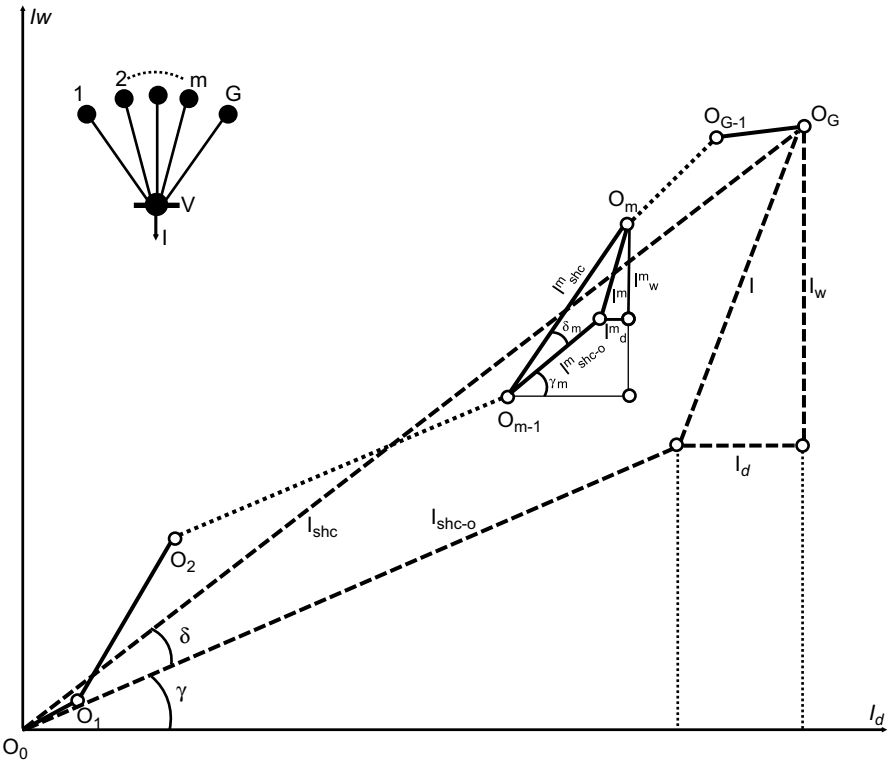

Fig. 2.8 Multiple generators connected to a bus via short-circuit admittances

$$\Sigma I_{dm} + \Sigma I_{shc-0m} \cos \gamma_m = I_d + \Sigma I_{shc-0m} \cos \gamma_m = \Sigma I_{shcm} \cos(\delta_m + \gamma_m). \tag{2.17}$$

In other words:

- The real component I_w of the total current flowing from generators to the load bus is equal to the sum of the full-load short-circuit currents projections on the ordinate axis minus the sum of the no-load short-circuit currents projections on the ordinate axis.
- The reactive component I_d of the total current flowing from generators to the load bus is equal to the sum of the full-load short-circuit currents projections on the abscissa axis minus the sum of the no-load short-circuit currents projections on the abscissa axis.

With the notations from Fig. 2.8 and remembering that V is the phase origin, the Eqs (16) and (17) can be rewritten as:

$$\underline{I} = \underline{I}_{shc} - \underline{I}_{shc-0} = \sum_m \underline{Y}_m \underline{E}_m - \left(\sum_m \underline{Y}_m + \underline{Y}_0 \right) V. \tag{2.18}$$

In addition to the information about currents and powers, the Nodal Image also provides information about voltages:

- The angles δ_m measure the angle between the phasors E_m and the voltage V, which is used as reference—therefore, the angle differences between the internal voltages of the generators retained in the model can be visualized by simply comparing their full-load short-circuit currents with the no-load short-circuit currents.
- The magnitude of the V voltage is proportional to the projection of the total full-load short-circuit current on the abscissa axis and may be measured by using a conveniently established scale.

Let us note that a generator injection represents an actual current only if the respective branch corresponds to a machine directly connected to the load bus. If this is not the case, the currents calculated with the previous formulae represent the contribution of each machine to the total current injected into the load bus. If similar REI Nets are built for all the load buses, the actual currents injected in generator buses can be calculated by adding the contributions of each generator node to the REI Nets.

Also important is the representation of generators. The base case is obtained from a load-flow calculation by modeling either the high-voltage busbars of the power stations, which is typical in planning studies, or the machine terminals, which is the current practice in real-time and study-mode network analysis as deployed in system operations. But neither approach can represent the *internal admittances* of the generators because, due to the ensuing emf values, which are higher or much higher than 1.0 pu, the load flow would diverge. Stability calculations, however, *must* take into account the behavior of the generators—otherwise, they would be meaningless.

Dimo solved this problem in a simple and elegant way. After the base case has been obtained, but prior to computing the short-circuit currents, the Y matrix is extended with the generators' internal admittances, which may correspond to synchronous reactances or some other reactance.

If synchronous reactances were used, the Nodal Images would give information about permanent short-circuit currents (without regulation) and about the "natural" stability of the system. For steady-state stability studies, where the effect of fast voltage controllers must be reflected, *the generators are represented through transient reactances*. Further details about the representation of generators are provided in the Sect. 3.4.2.

2.3.4 Reactive Power dQ/dV Stability Criterion

2.3.4.1 Exact, Algebraic and Practical Steady-State Stability Criteria

The conventional method of the small oscillations for estimating the steady-state stability (Anderson and Fouad 1990; Sauer and Pai 1990; Venikov 1977) consists of

examining the eigenvalues of the characteristic equation associated with the system of differential equations that describe the free transient processes after a small disturbance takes place in an automatically controlled power system.

The necessary and sufficient condition for steady-state stability is that all the real parts of the eigenvalues be negative (Venikov 1977, p. 216). The analysis encompasses the following steps:

- Describe the transient processes in the form of a system of nonlinear differential equations
- Linearize the equations around the solution point by expanding them into a Taylor series and retaining only the linear (first order) terms
- Calculate the main (characteristics) determinant and its minors and develop the characteristic equation
- Determine the sign of the real roots and the sign of the real part of the complex roots of the characteristic equation.

The approach is laborious and is replaced by determining relationships between the roots and the coefficients of the characteristic equation. Venikov calls these relations steady-state stability criteria (Venikov 1977, p. 216) and classifies them into *algebraic* (Routh–Hurwitz), *frequency-domain* (Nyquist), and *practical*.

A necessary condition for steady-state stability is derived from the Hurwitz criterion by evaluating the sign of the last term of the characteristic equation, which is the Jacobian determinant D. A change of sign from positive to negative (all Hurwitz determinants are positive) with further loading of the system indicates aperiodic instability. The instability in the form of self-oscillations, however, remains unrevealed by this method (Venikov 1977, p. 138).

If the generators are radially connected to a nodal point, and if, based on practical considerations, it may be assumed that some operating variables are constant, the condition $D=0$ leads to "practical criteria" that are valid within certain limits, for example, the *synchronizing power criterion* $dP/d\delta > 0$, which assumes constant frequency and constant voltage at the nodal point, and the *reactive power voltage and steady-state stability criterion* $dQ/dV < 0$, which assumes that the frequency is constant and the power balance is maintained at the load node (Venikov 1977, p. 138).

At the first sight, the requirement that the network be radial may seem impossible to meet, for power system transmission networks are never radial. However, Dimo recognized that the practical criteria match perfectly with the case of a power system network that has been replaced with an REI Net, which, in fact, *is* a radial network—not a radial network of physically identifiable admittances, except for the particular case of generators directly supplying a load, but *a radial network of short-circuit admittances connecting the system generators to a central node*. This is the case of both REI Nets built for actual load buses and REI Nets where all the system loads have been aggregated into a fictitious load bus, as shown in Fig. 2.9.

Dimo used the reactive power voltage and steady-state stability criterion $dQ/dV < 0$ in conjunction with the Nodal Image and obtained a simple and efficient

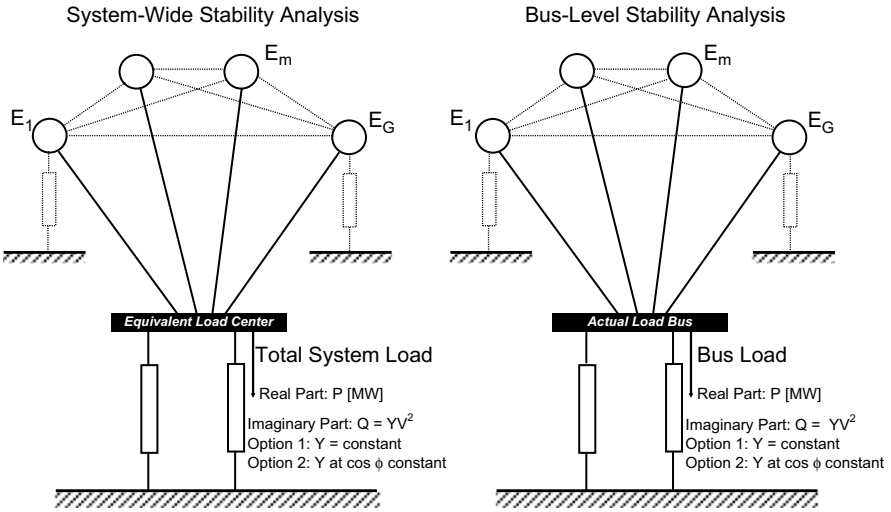

Fig. 2.9 Short-circuit current models for steady-state stability assessment

steady-state stability evaluation algorithm (Dimo 1961, 1975), which is described in detail in Sect. 3.4.4.

But before developing the general expression of Dimo's formulation of the reactive power voltage and steady-state stability criterion $dQ/dV < 0$, we need to discuss further aspects of generator and load modeling.

2.3.4.2 Modeling the Generators

Two approaches are possible for modeling the machines: representing in detail the excitation control systems, or using approximate models.

In planning studies where system alternatives must be explored in detail, e.g., when simulating past events that have actually occurred, or when developing protection schemes and operating criteria to maintain the power system stability, accurate modeling is necessary and requires detailed generator models. In the initial stages of such studies, though, or in operations planning studies, "simplified models may be adequate for real-time determination of operating limits and for some contingency analysis studies" (IEEE 1990).

The simplest model is the classical model, which consists of a constant voltage $E' = \text{const.}$ behind the transient reactance x'_d (IEEE 1990; Anderson and Fouad 1990; Venikov 1977; Dimo 1975). E' is determined from the pretransient conditions. During the transient condition, the magnitude E' is maintained constant while its angle δ is considered the angle between the rotor position and the voltage V on the machine's terminals.

As shown by Venikov, machines equipped with forced-action voltage controllers can be modeled as a constant voltage V and $x_{gen} = 0$ (Venikov 1977, pp. 214). Actually, this is how generators are represented, or, rather, *not* represented, in load-flow calculations, where the assumption is implicitly made that the generator bus voltages either at the machine terminals or on the high voltage side of the step-up transformer are and remain constant. In real life, however, these voltages are not constant and some "further constant voltage point must be found, such as the emf behind the synchronous reactance of an alternator" (Barbier and Barret 1980, p. 681).

Taking a more conservative approach, Dimo *always* represents the generators and, depending on how they are modeled, classifies the steady-state stability into "natural stability," in the absence of voltage regulation, and "artificial stability" if there is voltage regulation (Dimo 1975 p. 129). The natural stability is determined by extending the network with the synchronous reactances, whereas the artificial stability corresponds to the case where the network is extended with the transient reactances of the machines.

Relatively, recent research (Dobson and Liu 1993; Van Cutsem 1993) confirmed these early findings. Accordingly, generators that operate at the reactive power limits under light load conditions will cause the steady-state stability to decrease but not to be destroyed. At sufficiently high loadings, however, encountering the reactive power limits will immediately destabilize the system and precipitate a voltage collapse.

On this basis, an important extension of the original Dimo's method has been proposed (EPRI 1992/1993; Savulescu et al. 1993) and subsequently incorporated in the fast steady-state stability software documented in (Gonzalez 2003; Avila-Rosales et al. 2004; Savulescu 2004; Tweedy 2004; Avila-Rosales and Giri 2005; Vergara et al. 2005a; Campeanu et al. 2006; Virmani et al. 2007; Vickovic et al. 2009; Arnold et al. 2009; Eichler et al. 2011; Stottok et al. 2013).. It consists of simulating this behavior of the synchronous machine by changing its model from a constant emf E'_d behind the transient reactance x'_d to a constant emf E behind the synchronous reactance x_d when the reactive power at the machine terminals has reached the MVAr limit.

2.3.4.3 Modeling the Loads: Voltage Collapse and Dual Power States

Once a steady-state stable power-flow case has been obtained, the next step is to determine *how far* it is from instability. The limit, or critical state, is approached through a series of degraded states where, at each step, the generators produce more power and the bus voltage magnitudes become lower, until the point of voltage collapse is reached.

The results of this system stressing process, which is referred to as "case worsening," are affected significantly by how the loads have been represented. Three hypotheses can be made about modeling the load: constant admittance; constant *P* and *Q*; and a combination of the two.

Hypothesis 1: Load Modeled as $P=GV^2$ and $Q=BV^2$

Successive load increases cause the real powers flowing from generators into the study-bus to increase until the point of maximum power transfer, while the bus voltage magnitudes get smaller and smaller. Beyond that point, the power supply starts to decrease, the bus voltage continues to drop, and dual power states (same power at different voltages) are obtained. Ionescu and Ungureanu have demonstrated that, in this case, all the states are theoretically feasible, including the dual states, and a steady-state stability limit cannot be obtained (Ionescu and Ungureanu 1981; Ionescu 1993).

Hypothesis 2: Load Modeled as P=const and Q=const

In this case, the condition stated by the maximum power transfer theorem does correspond to the steady-state stability limit, and the dual states are unstable and have no physical meaning. This hypothesis is rigid and provides conservative results (Ionescu and Ungureanu 1981; Ionescu 1993).

Hypothesis 3: Load Modeled as P=const and $Q=BV^2$

This hypothesis, which was used extensively by Dimo, implies that the real part of the load does not vary with the bus voltage, and that the reactive component of the load can be represented as a fixed susceptance. This model implies that, while the real power increases, the load's susceptance is maintained constant and a reduction of the bus voltage implies a reduction of the reactive power. In this case, the state associated with the maximum power transfer is critical and occurs when $dQ/dV = 0$.

This model can further be refined by considering that the reactive power of the load varies proportionally with the power factor in the base case. If we note the power factor of the load in the base case with $\tan\varphi_{bc}$, the reactive part of the load for the base case is given by

$$Q_{bc} = P\tan\varphi_{bc} = BV_{bc}^{\ 2}, \tag{2.19}$$

and the load's susceptance at different values of P [MW] can now be recomputed with formula (20)

$$B = \frac{P\tan\varphi_{bc}}{V_{bc}^{\ 2}}. \tag{2.20}$$

With the notation, $c_{bc} = \tan\varphi_{bc}/V_{bc}^{\ 2}$, where c_{bc} is constant, we get:

$$Q = c_{bc}PV^2 \tag{2.21}$$

The formulation (2.21) of Hypothesis 3 corresponds to an average scenario and is well suited for steady-state stability simulations.

2.3.4.4 General Expression of Dimo's Formulation of the Reactive Power Voltage and Steady-State Stability Criterion

As shown in Sect. 3.4.1, the only assumption required to apply the reactive power voltage and steady-state stability criterion to the case of a slow and small variation of the voltage or of the reactive power at a bus connected radially to generators through short-circuit admittances is for the system frequency to be maintained constant (Venikov 1977). In order to build the REI Net and the associated Nodal Image, we start from a solved base case and, then, extend the network with the internal reactances of the generators in accordance with the criteria discussed in Sect. 3.4.2.

When performing a system-wide stability study, all the system loads are aggregated into a single load center as shown in Fig. 2.6. If we perform a bus-level analysis, the study-bus is retained with its actual identity. In either case, the real and reactive parts of the load at the central node of the REI Net are modeled as shown in Fig. 2.9 and in accordance with Hypothesis 3 in Sect. 3.4.3.3.

Dimo derived his version of the dQ/dV criterion for a Nodal Image associated to an REI Net of *reactances,* in which case the angles γ_m in Fig. 2.8 are equal to zero. In the following, we will prove the reactive power voltage and steady-state stability criterion for *the general case,* and then, by substituting $\gamma = 0$, we will obtain the original Dimo's formula.

Let us consider an REI Net with *n* generators. The total real and reactive powers supplied by these machines are:

$$P_g = P_1 + P_2 + \ldots + P_n \tag{2.22}$$

$$Q_g = Q_1 + Q_2 + \ldots + Q_n, \tag{2.23}$$

and, by using the relationships (10) and (11), the Eqs (2.22) and (2.23) may be written as:

$$\begin{aligned} P_g = {} & Y_1 E_1 V \sin(\delta_1 + \gamma_1) + Y_2 E_2 V \sin(\delta_2 + \gamma_2) + \ldots \\ & + Y_n E_n V \sin(\delta_n + \gamma_n) - Y_1 V^2 \sin\gamma_1 - Y_2 V^2 \sin\gamma_2 - \ldots - Y_n V^2 \sin\gamma_n \end{aligned} \tag{2.24}$$

$$\begin{aligned} Q_g = {} & Y_1 E_1 V \cos(\delta_1 + \gamma_1) + Y_2 E_2 V \cos(\delta_2 + \gamma_2) + \ldots \\ & + Y_n E_n V \cos(\delta_n + \gamma_n) - Y_1 V^2 \cos\gamma_1 - Y_2 V^2 \cos\gamma_2 - \ldots - Y_n V^2 \cos\gamma_n \end{aligned} \tag{2.25}$$

the reactive load being given by

$$Q_l = Y_l V^2. \tag{2.26}$$

Applying the dQ/dV criterion (Venikov 1977, pp. 138–139) to Eqs (2.25) and (2.26), we obtain:

$$\frac{dQ}{dV}=\frac{d(Q_g-Q_l)}{dV}=Y_1E_1\cos(\delta_1+\gamma_1)+Y_2E_2\cos(\delta_2+\gamma_2)+\ldots+Y_nE_n\cos(\delta_n+\gamma_n)$$
$$-Y_1E_1V\sin(\delta_1+\gamma_1)\frac{\partial\delta_1}{\partial V}-Y_2E_2V\sin(\delta_2+\gamma_2)\frac{\partial\delta_2}{\partial V}-\ldots$$
$$-Y_nE_nV\sin(\delta_n+\gamma_n)\frac{\partial\delta_n}{\partial V}-2Y_1\cos\gamma_1V-2Y_2\cos\gamma_2V-\ldots-2Y_n\cos\gamma_nV-2Y_lV. \tag{2.27}$$

The partial derivatives $\partial\delta_1/\partial V,\ldots,\partial\delta_n/\partial V$ are obtained from Eq (2.10) by considering that the real powers are constant (Hypothesis 3, Sect. 3.4.3.3) and the angles $\gamma_1,\gamma_2,\ldots,\gamma_n$ do not depend upon V

$$\frac{dP_1}{dV}=0=Y_1E_1\sin(\delta_1+\gamma_1)+Y_1E_1V\cos(\delta_1+\gamma_1)\frac{\partial\delta_1}{\partial V}-2Y_1\sin\gamma_1V \tag{2.28}$$

$$\frac{dP_n}{dV}=0=Y_nE_n\sin(\delta_n+\gamma_n)+Y_nE_nV\cos(\delta_n+\gamma_n)\frac{\partial\delta_n}{\partial V}-2Y_n\sin\gamma_nV, \tag{2.29}$$

whence

$$\frac{\partial\delta_1}{\partial V}=\frac{2V\sin\gamma_1-E_1\sin(\delta_1+\gamma_1)}{E_1V\cos(\delta_1+\gamma_1)} \tag{2.30}$$

$$\frac{\partial\delta_n}{\partial V}=\frac{2V\sin\gamma_n-E_n\sin(\delta_n+\gamma_n)}{E_nV\cos(\delta_n+\gamma_n)}. \tag{2.31}$$

By substituting Eqs (2.30) and (2.31) in Eq (2.27), we obtain:

$$\frac{dQ}{dV}=\frac{Y_1E_1}{\cos(\delta_1+\gamma_1)}+\frac{Y_2E_2}{\cos(\delta_2+\gamma_2)}+\ldots+\frac{Y_nE_n}{\cos(\delta_n+\gamma_n)}$$
$$-2\left[Y_1\frac{\sin\gamma_1\sin(\delta_1+\gamma_1)}{\cos(\delta_1+\gamma_1)}+\ldots+Y_n\frac{\sin\gamma_n\sin(\delta_n+\gamma_n)}{\cos(\delta_n+\gamma_n)}\right]V$$
$$-2(Y_1\cos\gamma_1+Y_2\cos\gamma_2+\ldots+Y_n\cos\gamma_n+Y_l)V, \tag{2.32}$$

and, with the notation (2.33)

$$Y^{\gamma}=Y_1\sin\gamma_1\tan(\delta_1+\gamma_1)+Y_2\sin\gamma_2\tan(\delta_2+\gamma_2)+\ldots+Y_n\sin\gamma_n\tan(\delta_n+\gamma_n), \tag{2.33}$$

we obtain the *general expression of Dimo's formulation of the reactive power voltage and steady-state stability criterion*:

$$\frac{dQ}{dV} = \sum_m \frac{Y_m E_m}{\cos(\delta_m + \gamma_m)} - 2\left(\sum_m Y_m \cos\gamma_m + Y_l + Y^{\gamma}\right)V. \tag{2.34}$$

If the REI Net branches are approximated through pure reactances, i.e., if $\gamma_1 = \gamma_2 = ... = \gamma_n = 0$, we get the *original formulation of Dimo's reactive power voltage and steady-state stability criterion* (Dimo 1961., 1977)

$$\frac{dQ}{dV} = \sum_m \frac{Y_m E_m}{\cos\delta_m} - 2\left(\sum_m Y_m + Y_l\right)V \tag{2.35}$$

2.3.4.5 Distance to Instability: The Case-Worsening Procedure

In voltage and steady-state stability problems, it is *not the base case,* which presumably comes from a fully converged load flow or state estimate, that is of primary importance, since, in most cases, the base case is stable. What really counts is the ability to characterize the system state by its "distance" from an unstable one.

The steady-state stability calculations *per se,* either via simplified techniques such as practical stability criteria or based on detailed simulation, e.g., evaluating the eigenvalues of the Jacobian associated with the system of dynamic equations, would not give such information. In order to find the distance to instability, the steady-state stability calculation must be combined with a "system stressing," or "case-worsening," procedure, whereby various system parameters are changed in a direction that is unfavorable to stability.

When using Dimo's methodology, there are several ways to perform case worsening *without* having to recalculate the base case load flow:

- Increase the total generated power to supply successively increased MW load levels—this is achieved by rotating the Nodal Image vectors anticlockwise (trigonometrically) and, as far as the load model is concerned, by considering that the reactive load is modeled by a susceptance that either:
- has a fixed value, as per Hypothesis 3 in Sect. 3.4.3.3 or
- varies proportionally with the power factor in the nominal (base) case, as per Eq (21) in Sect. 3.4.3.3.
- Represent the loss of excitation on one or several machines—on the Nodal Image, this is done by reducing the length (module) of the short-circuit currents of the generators.
- Sudden change of the operating conditions of generators that have reached the reactive power limits—if this happens under
- light load conditions, replacing the transient reactance with the synchronous reactance will cause the steady-state stability to decrease but not to be destroyed.
- high loadings, the same machine model change may destabilize the system and precipitate a voltage collapse.

Some structural changes can also be simulated on the Nodal Image, for example, adding or removing capacitor banks. But if the network changes are significant, e.g., after single and/or multiple line and/or generator contingencies, a new load-flow solution is required to correctly apply Dimo's technique. Once the new base case has been calculated, the REI Net and the Nodal Image are updated and, then, the steady-state stability index and distance to instability for the new system state are evaluated.

Another situation appears frequently in power systems where, due to specific network topology and load characteristics, significant reactive compensation resources, such as shunt capacitors and MVAr generating units, must be brought on line during peak-load conditions in order to maintain an "adequate" system voltage profile, "adequate" meaning that the bus voltages are sufficiently high to preclude the risk of blackout.

When the same power system operates at medium and light load levels, the reactive compensation goes the other way—capacitors are removed, shunt reactors are reconnected, synchronous condensers and/or units that were running essentially for generating MVArs are taken off-line, and major high-voltage transmission lines are disconnected.

It is obvious that during peak-load conditions, such operating procedures push the network's "maximum loadability," i.e., its steady-state stability limit, at values much higher than the maximum loadability at medium and light load levels. Accordingly, the voltage and steady-state stability calculations should be initiated from different base cases, each one reflecting the structurally different operating scenarios. A fine example that illustrates this situation is described in the reference Vergara et al. (2005).

2.3.4.6 P–V Relationship at the Study Bus

As indicated in Sect. 3.2, the short-circuit current's model has been used extensively in the voltage stability literature to develop power–voltage relationships at load buses. Two references come immediately to mind: the Appendix of Barbier and Barret (1980) and the paper by Ionescu and Ungureanu(1981). The former calculates the critical voltage at the study bus by assuming that the load is modeled as a constant impedance, whereas the later discusses $P = f(V)$ P–V relationship for a network of reactances when the load is represented as per Hypothesis 3 in Sect. 3.4.3.3. In both cases, it is assumed that the voltages at the generator buses are constant, i.e., they correspond to the emf behind some internal generator reactance.

In the following, we will generalize Ionescu and Ungureanu's approach and develop a $P = f(V)$ function for a network of complex admittances with a load $P + jQ$ at the study bus, with Q given by Eq (2.21). In order to simplify the notations, the formula will be initially developed for an elementary REI Net (Fig. 2.7), then it will be extended for the general case.

Let us consider again the Eqs (2.8) and (2.9) and, using (2.21) to express Q as a function of P and V^2, rewrite them as follows:

$$\frac{P + YV^2 \sin\gamma}{YEV} = \sin(\delta + \gamma) \tag{2.36}$$

$$\frac{c_{\text{bc}} V^2 P + YV^2 \cos\gamma}{YEV} = \cos(\delta + \gamma). \tag{2.37}$$

By eliminating δ between Eqs (2.36) and (2.37), we obtain:

$$(P + YV^2 \sin\gamma)^2 + (c_{\text{bc}} V^2 P + YV^2 \cos\gamma)^2 = Y^2 E^2 V^2, \tag{2.38}$$

then

$$(1 + c_{\text{bc}}{}^2 V^4) P^2 + 2P(YV^2 \sin\gamma + c_{\text{bc}} YV^4 \cos\gamma) = Y^2 E^2 V^2 - Y^2 V^4. \tag{2.39}$$

With the notations (2.40) and (2.41)

$$A = \frac{YV^2(\sin\gamma + c_{\text{bc}} V^2 \cos\gamma)}{1 + c_{\text{bc}}^2 V^4} \tag{2.40}$$

$$B = \frac{Y^2 V^4 \left(\frac{E^2}{V^2} - 1\right)}{1 + c_{bc}{}^2 V^4}, \tag{2.41}$$

Eq (2.39) can be successively be rewritten as:

$$P^2 + 2PA = B$$

$$P^2 + 2PA + A^2 = B + A^2$$

$$P = -A + \sqrt{B + A^2}.$$

By effecting all the substitutions and algebraic manipulations, we finally obtain the $P = f(V)$ function that expresses the relationship between the power supplied by a generator to a bus and the voltage at that bus

$$P = f(V) = \frac{YV^2}{1 + c_{bc}{}^2 V^4}[-c_{bc} V^2 \cos\gamma - \sin\gamma + \sqrt{(1 + c_{bc}{}^2 V^4)\left(\frac{E^2}{V^2} - 1\right) + (\sin\gamma + c_{bc} V^2 \cos\gamma)^2}\,]. \tag{2.42}$$

With the substitution $\gamma = 0$, which corresponds to the case of a generator connected to a load through a reactance, e.g., a high-voltage transmission line with resistance practically equal to zero, we obtain the formula developed by Ionescu and Ungureanu in Ionescu and Ungureanu (1981)

$$P = f(V) = \frac{YV^2}{1 + c_{bc}{}^2 V^4}\left[-c_{bc}V^2 + \sqrt{\frac{E^2}{V^2}(1 + c_{bc}{}^2 V^4) - 1}\right]. \tag{2.43}$$

Formula (2.42) can easily be generalized to relate the voltage V of a bus, where the power P is supplied by $1,...,m,...,n$ generators with internal voltages $E_1,...,E_m,...E_n$ through an REI Net of complex admittances $Y_1\underline{|-\varphi_1}, ..., Y_m\underline{|-\varphi_m}, ..., Y_n\underline{|-\varphi_n}$, with $\gamma_1 = 90^\circ - \varphi_1, ..., \gamma_m = 90^\circ - \varphi_m, ..., \gamma_n = 90^\circ - \varphi_n$

$$\begin{aligned} P_\Sigma = \sum_m \{ & \frac{Y_m V^2}{1 + c_{bc}{}^2 V^4}[-c_{bc}V^2 \cos\gamma_m - \sin\gamma_m \\ & + \sqrt{(1 + c_{bc}{}^2 V^4)\left(\frac{E_m{}^2}{V^2} - 1\right) + (\sin\gamma_m + c_{bc}V^2\cos\gamma_m)^2}\,]\}. \end{aligned} \tag{2.44}$$

When applying the formula (2.44), it must be remembered that the

- Powers P_m that flow from generators towards the load bus enter the branches of the REI Net *after* the equivalent shunts near the generator buses (Figs. 2.4 and 2.5) and reach the point *i* (Fig. 2.5) *before* the equivalent shunt $Y_i 0$. In other words, the total power supplied by generators to the study bus covers both the load and whatever shunts resulted after linearizing and eliminating all the other load buses.
- Internal reactances of the generators must be included in the model *after* the load-flow case has been calculated but *before* reducing the system to the REI Net.

2.4 Practical Considerations

2.4.1 Visualization Capabilities of Nodal Images

Dimo used Nodal Images to characterize the power system structure and operating conditions: "Once the network representation has been established, a more general characterization of it can be achieved with the help of the geometry of the resulting Nodal Images. For example, a Nodal Image built for an arbitrary node allows grasping the interdependence between the represented node and every other node retained in the REI Net. The aspect of the vector which appears in the chain composing the vector of the short-circuit current, compared with the resultant vector and with the other component vectors, supplies the necessary indications" (Dimo 1975).

In the following, we will focus on the ability to extract *information* from the results of steady-state stability analysis calculations and, using the Nodal Image analogy, to display the results in graphical formats suitable for use with modern computing technologies.

2.4.2 Displaying the Results of Steady-State Stability Calculations

2.4.2.1 Distance to Instability and Security Margin. Steady-State Stability Reserve

The search for the steady-state stability limit begins with a Nodal Image for the base case and continues by rotating the chain of vectors in trigonometric sense until dQ/dV becomes positive. The state immediately before instability is called critical state. Once the critical state has been obtained, the security margin is calculated by reversing the case-worsening algorithm and "derotating" the Nodal Image until the system full-load short circuit current vector projection on the ordinate axis becomes equal to, or smaller than, a predefined threshold, e.g. 15% below the critical state.

The angle between the system full-load short circuit current vector in the base case and the system full-load short circuit current vector in the critical state measures the distance to instability. These vectors can be mapped on a *speedometer chart* normalized on a 90°-wide proportional scale where the system state is represented by a *needle* situated between 0°, corresponding to 0 MW, and 90°, which corresponds to instability.

If the security margin MW is also shown on the speedometer, the area between it and the critical MW depicts the set of potentially unsafe operating states, whereas the area to its left corresponds to states where there is no risk of instability.

If the needle's position maps the value of the dQ/dV derivative rather than the amount of generated MW, a nonproportional scale speedometer is obtained. On this type of speedometer, the needles corresponding to two different system states with the same total MW generation but different dQ/dV values would be shown at different distances from instability. The linear (MW) and nonlinear (dQ/dV) speedometers can be combined on a *two-speedometer* chart, as shown in Fig. 2.10.

This ergonomically powerful representation embodies the *stability envelope* concept illustrated in Fig. 2.2, where the "safe" operating region is shown in green (or blue on the dQ/dV speedometer) and corresponds to system MW grid utilization values smaller than the MW security margin. Let us also note that the red sector does not depict an operating area for the very simple reason that, after instability, a system state would not exist: it is blackout, so there would be no system state any longer.[7]

[7] Technically speaking, the "red area" should have been just a thin line; however, for ergonomic reasons, it is shown with some depth so that it could be easily identified on the display. Accordingly, for the speedometers in Fig. 2.10, the distance to instability is conveyed by the position of

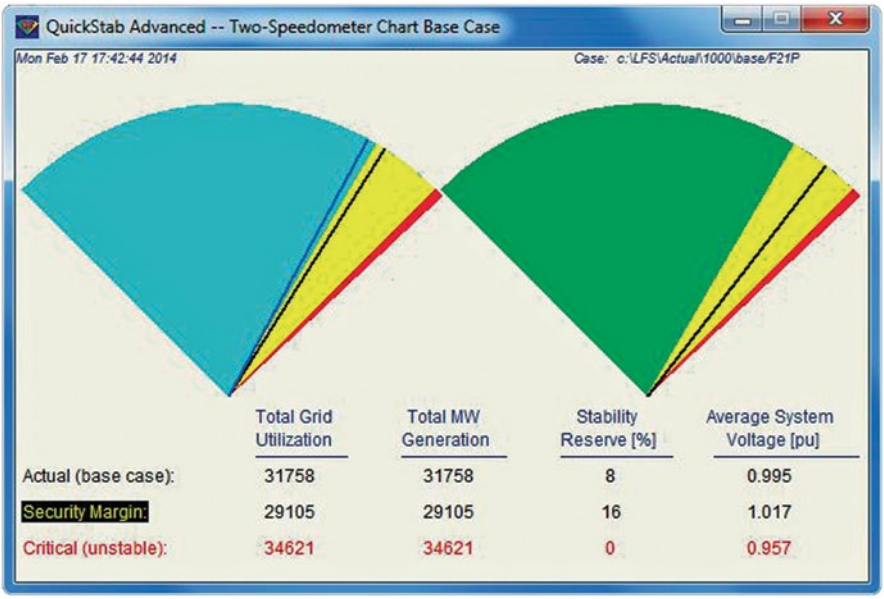

Fig. 2.10 Two-speedometer chart depicting base case system conditions. The *left-hand* speedometer is rated in dQ/dV units whereas the *right-hand* speedometer is rated in MW

Figure 2.11 illustrates a two-speedometer chart where the base case and the worst contingency case, respectively, are represented side by side.

As opposed to the Nodal Image, which requires a thorough familiarity with the theoretical background that substantiates the visualization of system states via short-circuit current vectors, the speedometer charts make it possible to *see,* and instantly evaluate, both how far a system state is from instability and how far it is from the security margin—without reading numbers, and without the need to understand the underlying technology. Furthermore, the speedometer charts facilitate the comparison between different system states and, just through the movement of the needles, allow monitoring the system evolution towards, or away from, instability.

2.4.2.2 Impact of Generators on Steady-State Stability. System-Wide and Bus-Level Unit Ranking

Another capability of the Nodal Image is its ability to show which generators are important and how they impact the steady-state stability of the system, in system-wide analysis, or of the load-bus, in bus-level calculations. For example, a short-circuit current vector that is negligible with respect to the module of the resultant

the needle with respect to the left edge of the red sector and, on the right-hand speedometer, is quantified by the stability reserve below the SSSL.

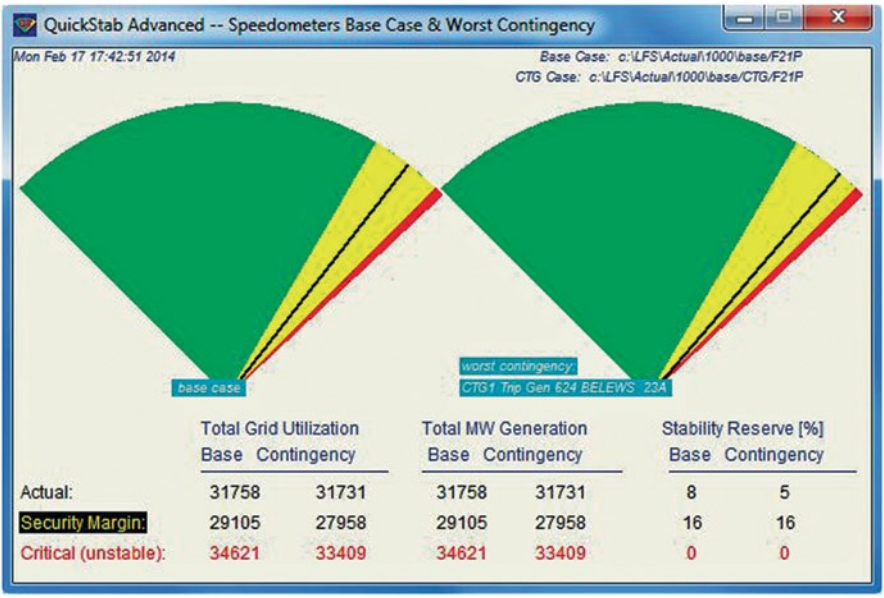

Fig. 2.11 Two-speedometer chart depicting a contingency case developed from the base case conditions shown in Fig. 2.10. Note how the *black needle* has moved to the right, thus indicating that the system's steady-state stability reserve has decreased

vector and has a small angle corresponds to a machine that has little or no effect upon the bus that is being investigated.

The *unit impact bar chart* illustrated in Fig. 2.12 is built from the information conveyed by the Nodal Image. It depicts the impact of synchronous machines, SVCs, tie-line injections, etc. on the system's steady-state stability conditions in the *descending order of the normalized values of* $Y_m E_m / \cos \delta_m$.

2.4.3 Real-Time Implementation

At the outset, it is important to define what is actually meant by "real time." For instance, an application may use real-time input but, due to lengthy calculations, may not be able to converge quickly enough for the results to be used online. This, of course, is not quite … real-time.

On the other hand, an application that is fast enough to produce real-time results and graphics from real-time input can be implemented in two ways:

- *Seamlessly integrated* with the Supervisory Control And Data Acquisition/Energy Management System (SCADA)/EMS, i.e., executing on the application servers and triggered, automatically, upon event and/or operator request, by the real-time scheduler of the SCADA/EMS system.

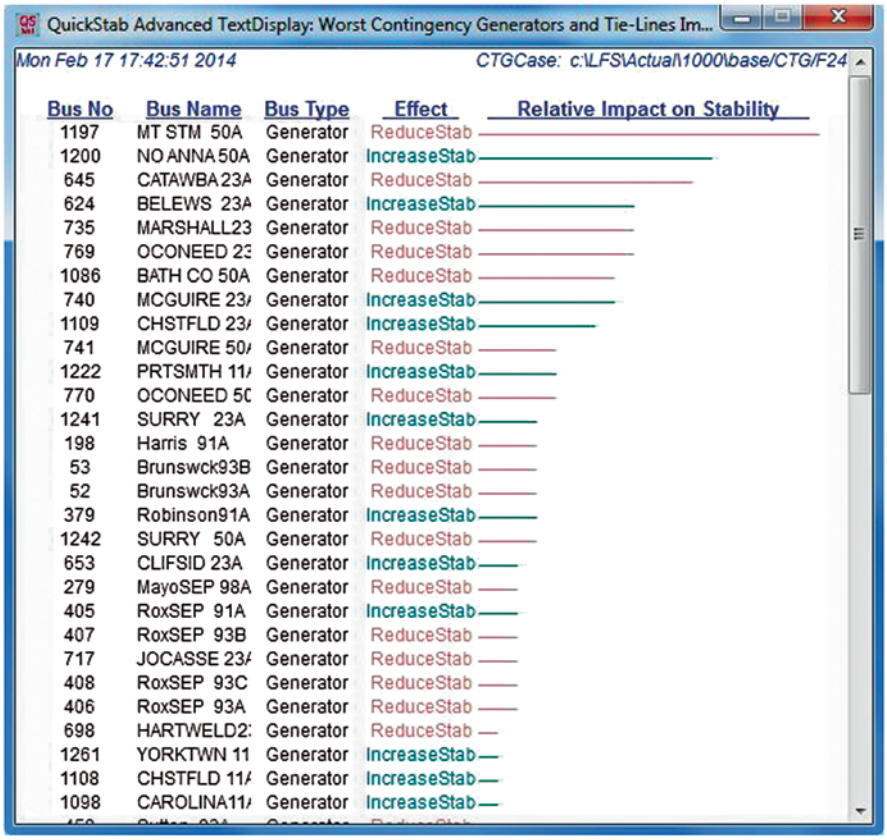

Fig. 2.12 Unit ranking chart. The generators are shown in the order of their impact on the system-wide steady-state stability conditions

- *In parallel* with the real-time system, i.e., using real-time data computed on the SCADA/EMS but running on an off-line processor.

Due to its remarkable solution speed, the steady-state stability assessment technique described in this chapter has been both seamlessly integrated on SCADA/EMS servers and used on off-line processors with state estimation results imported from the real-time system.

Figure 2.13 depicts the early seamless integration of this tool with third-party SCADA/EMS installations. Updated information about the current implementation and use of Siemens Spectrum Power QuickStab is provided in the Chap. 4 of this book (Eichler et al. 2014).

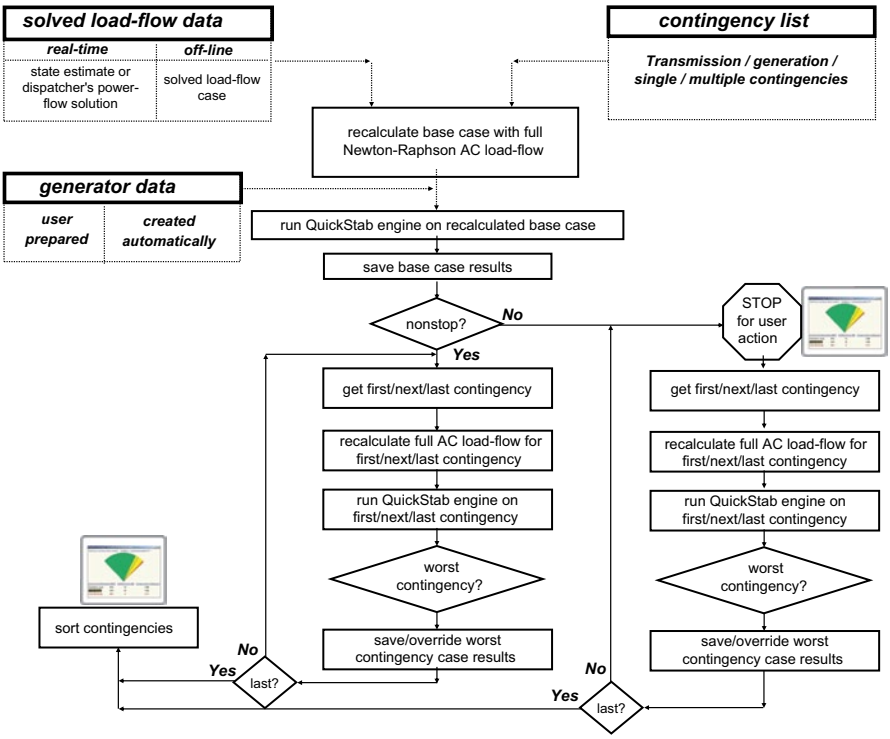

Fig. 2.13 Seamless SCADA/EMS integration of the fast steady-state stability tool

2.5 Conclusions

The main purpose of this chapter was to set the stage for the use of steady-state stability analysis tools to compute the risk of steady-state instability in real time. The approach was illustrated with a field-proven technique that has been successfully deployed in multiple SCADA/EMS installations to assess the power system's distance to instability both in real time, in conjunction with state estimators, and off-line, with conventional power-flow programs.

The method, inspired from Paul Dimo's steady-state stability assessment method, determines quickly and reliably how far the transmission network is from a state where voltages may collapse and units may lose synchronism.

The underlying assumptions were extensively analyzed and their validity was substantiated. For the theoretically oriented reader, this chapter also included the detailed development of the generalization of Dimo's formulation of the reactive power steady-state stability criterion, and an extension of the $P = f(V)$ relationship for the case where the bus loads are modeled as $P + j\,Q$, rather than constant impedances, and their reactive parts vary proportionally with the power factor in the nominal (base) case.

Both the theoretical analysis and the actual implementation experience, including accuracy and validity tests performed in several control centers, which are summarized in Chap. 3 of this book, point to a mandatory tool for the online computation and monitoring of the distance to instability.

Acknowledgement The display pictures shown in Fig. 2.10 through 2.13 have been provided by and used with permission from Siemens AG, Nuremberg, Germany.

References

Anderson PM, Fouad AA (1990) Power system control and stability. Iowa University Press, Ames

Arie E, Pomarleanu M, Bejuscu L, Botgros M (1973) Determinarea Rezervei de Stabilitate Statica a Sistemelor Electroenergetice Complexe, Studii Èi Cercetari de Energetica si Electrotehnica, Tom 23, Nr. 3, pp 709–727, Bucharest, Romania, 1973

Arnold L, Hajagos J, Manessis SM, Philip A (2009) LIPA implementation of real-time stability monitoring in a CIM compliant environment. In: Savulescue SC (ed) Real-time stability assessment in modern power system control centers. Wiley, New York

Avila-Rosales R, Giri J (2005) Wide area control for more reliable operation of the power system grid. In: Savulescu SC (ed) Real time stability in power systems. Springer, Norwell

Avila-Rosales R, Giri J, Lopez R (2004) Extending EMS capabilities to include on-line stability assessment. Paper 04PS0371 presented at the real-time stability challenge panel session, power systems conference and exposition 2004, New York, 10–13 Oct 2004

Barbier C, Barret JP (1980) An analysis of phenomena of voltage collapse on a transmission system. Rev Gén Electr 89(7):3–21

Campeanu HS, L'Helguen E, Assef Y, Vidal N, Savulescu SC (2006) Real-time stability monitoring at transelectrica. Paper PSCE06–1288 presented at the real-time stability applications in modern SCADA/EMS panel, IEEE power systems conference & exposition 2006 (IEEE PSCE'04), Atlanta, October 29–November 2, 2006

Crary SB (1945) Power system stability. General Electric Series. Wiley, New York. (Copyright 1945, Third Printing October 1955)

Dimo P (1961) Etude de la stabilité statique et du réglage de tension. Rev Gén Electr 70(11):552–556

Dimo P (1962) L'Analyse des réseaux d'énergie par la méthode nodale des courants de court-circuit. L'image des noeuds. Rev Gén Electr 71:151–175

Dimo P (1968) Nodal analysis of electrical power systems (Romanian edition), Editura Academiei, Bucharest

Dimo P (1975) Nodal analysis of power systems. Abacus, Kent

Dimo P, Manolescu G, Iordanesscu I, Groza L, Ionescu S, Albert H, Moraite G, Ungureanu B (1971) Computation and design of electrical energy systems (Romanian edition), Editura Tehnica, Bucharest, pp 200–201

Dobson I, L. Liu (1993) Immediate change in stability and voltage collapse when generator reactive power limits are encountered. In: Fink LH (ed) Proceedings of international seminar on bulk power system voltage phenomena II. ECC, Virginia, pp 65–74

DyLiacco TE, Savulescu SC, Ramarao KV (1978) An on-line topological equivalent for a power system. IEEE Trans Power Appar Syst PAS-97(9): 1550–1563

Eichler R, Krebbs R, Savulescu SC, Wache M (2011) Early detection and mitigation of the risk of blackout (co-author). Paper presented at CIGRE international symposium "The Electric Power System of the Future—Integrating Supergrids and Microgrids in Transmission Grid Operation", Bologna, Italy, 13–15 Sept 2011

Eichler R, Heyde CO, Stottok BO (2014) Composite approach for the early detection, assessment and visualization of the risk of instability in the control of smart transmission grids, real-time stability in power systems, 2nd edn. Springer, New York

EPRI (1992/1993) Power system steady-state stability monitor prototype. Final report EPRI TR-100799, July 1992. and Power system steady-state stability monitor, final report EPRI TR-103169, Dec 1993

EPRI (1992) VSTAB voltage stability analysis program, final report, RP3040–1, Electric Power Research Institute, Sept 1992

Erwin SR, Oatts ML, Savulescu SC (1994) Predicting steady-state instability. IEEE Comput Appl Power 4(7):15–22

Gonzalez LA (2003) Post-facto analysis of a near-blackout event, 7th international workshop on power control centers, Orisei, Italy, 26–28 May 2003

IEEE (1982) PES task force on terms and definitions, proposed terms and definitions for power system stability. IEEE Trans Power Appar Syst PAS-101(7):1894

IEEE (1990) Guide for synchronous generator modeling practices in stability analysis, PES Publication P1110/D11 sponsored by the Joint Working Group on determination and application of synchronous machine models for stability studies, May 1990

IEEE/CIGRE (2004) IEEE/CIGRE joint task force on stability terms and definitions, definition and classification of power system stability. IEEE Trans Power Syst 19(2):1387–1401

Ionescu S (1993) Discussion of the paper fast steady-state stability assessment for real-time and operations planning. IEEE Trans Power Syst 8(4):1557–1569

Ionescu S, Ungureanu B (1981) The dual power states and voltage collapse phenomena. Rev Roum Sci Tech, Série Electrotech Energ 26(4):545–562

Kundur P (1999) Introduction to techniques for power system stability search. A special publication of the power system dynamic performance committee of the IEEE PES, TP-138-0, pp 1–3

Kundur P, Morison GK (1993) Classes of stability in today's power systems. IEEE Trans Power Syst 8(3):1159–1171

Magnien M (1964) Rapport spécial du Groupe 32 Conception et Fonctionnement des Réseaux. Conférence Internationale des Grands Réseaux Electriques Ã Haute Tension, CIGRE Session 1964

Moraite G, Ionescu S, Feldmann S, Chenzbraun I (1966) Problèmes soulevés par la stabilité statique des réseaux bouclés. Conférence Internationale des Grands Réseaux Electriques Ã Haute Tension, CIGRE Session 1966

Morison K, Wang L, Kundur P, Lin Xi Gao W, He C, Xue F, Xu T, Xu J, Xue Y (2004) Critical requirements for successful on-line security assessment. Paper presented at the real-time stability challenge panel session, power systems conference and exposition 2004, New York 10–13 Oct 2004

Navarro-Perez R, Prada RB (1993) Voltage collapse or steady-state stability limit. In: Fink LH (ed) Proceedings of international seminar on bulk power system voltage phenomena II. ECC, Virginia, pp 75–84

NERC (1996) Available transfer capability definitions and determination, North American Electric Reliability Council, June 1996

NERC (2000) Policy 9—Reliability coordinator procedures, Version 2, approved by Board of Trustees, Feb 7, 2000

Oatts ML, Erwin SR, Hart JL (1990) Application of the REI equivalent for operations planning analysis of interchange schedules. IEEE Trans Power Appar Syst PAS-109(5):547–555

Sauer PW, Pai MA (1990) Power system steady-state stability and the load-flow Jacobian. IEEE Trans Power Syst 5(4):1374–1381

Savulescu SC (1981) Equivalents for security analysis of power systems. IEEE Trans Power Appar Syst Pas-100(5):2672–2682

Savulescu SC (2004) A metric for quantifying the risk of blackout. Paper 04PS0294 presented at the real-time stability challenge panel session, power systems conference and exposition 2004, New York, 10–13 Oct 2004

Savulescu SC, Oatts ML, Pruitt JG, Williamson F, Adapa R (1993) Fast steady-state stability assessment for real-time and operations planning. IEEE Trans Power Syst 8(4):1557–1569

Stottok BO, Heyde CO, Eichler R, Savulescu SC (2013) Visualizing the risk of blackout in smart transmission grids (co-author). Paper presented at CIGRE international symposium "Smart grids: next generation grids for new energy trends", Lisbon, Portugal, April 2013

Tinney WF, Powell WI (1977) The REI approach to power network equivalents, PICA'77 conference, Toronto, Canada, May 1977

Tweedy J (2004) Assessing stability conditions to evaluate the risk of blackout. A real-time indicator based on field-proven techniques, Transmission and Distribution, June 2004, pp. 622–628

Van Cutsem Th (1993) Voltage collapse mechanisms—a case study. In: Fink LH (ed) Proceedings of international seminar on bulk power system voltage phenomena II. ECC, Virginia, pp 85–102

Venikov VA (1977) Transient processes in electrical power systems. Stroyev VA (ed), English Translation, MIR, Moscow

Venikov VA, Stroev VA, Idelchick VI, Tarasov VI (1975) Estimation of electrical power system steady-state stability. IEEE Trans Power Appar Syst 94(3):1034–1041

Vergara JS, Thai TA, Cuong ND, Nam NT, Campeanu HS, Savulescu SC (2005) Accuracy testing and real-time implementation of Dimo's stability analysis technique. In: Savulescu SC (ed) Real-time stability in power systems. Springer, Norwell

Vickovic D, Eichler R (2009) Real-time stability monitoring at the independent system operator in Bosnia and Herzegovina. In: Savulescu SC (ed) Real-time stability assessment in modern power system control centers. Wiley, New York

Virmani S, Vickovic D, Savulescu SC (2007) Real-time calculation of power system loadability limit. Paper no. 576 presented at the Powertech 2007 conference, Lausanne, Switzerland, 1–5 July 2007

Vournas CD, Sauer PW, Pai MA (1996) Relationships between voltage and angle stability of power systems. Electr Power Energy Sys 18(8):493–500

Wu FF, Narasimhamurti N (1979) Necessary conditions for REI reduction to be exact. IEEE PES winter meeting 1979, Paper A 79 065–4